POLITECNICO DI TORINO
Repository ISTITUZIONALE

High-frequency nonlinear vibration analysis through low-frequency stereo-camera systems

(Article begins on next page)

05 February 2025

High-frequency nonlinear vibration analysis through low-frequency stereo-camera systems

Daniele Botto [a],[*], Serena Occhipinti [a], Christian Maria Firrone [a], Paolo Neri [b]

[a] *Department of Mechanical and Aerospace Engineering, Politecnico di Torino, Corso Duca degli Abruzzi 24, Torino, 10129, Italy*
[b] *Department of Civil and Industrial Engineering, Universitá di Pisa, Largo L. Lazzarno 1, Pisa, 56122, Italy*

ARTICLE INFO

ABSTRACT

This paper describes a new methodology that expands the capabilities of low-frame, high-resolution stereo-camera systems in studying the dynamic behavior of components in the presence of nonlinear phenomena. A new downsampling technique called the Smoothed Harmonics Analysis (SHA) is proposed. This technique addresses the limitations due to the low-frame rate cameras for the study of high-frequency periodic steady-state nonlinear oscillations. SHA enables accurate reconstruction of downsampled signals, thus opening up numerous potential applications. The feasibility of this technique is demonstrated by analyzing the motion of a beam with nonlinear behavior. The nonlinearity is caused by intermittent contact while the beam is subjected to harmonic excitation.

1. Introduction

1.1. Background and motivation

Non-contact measurement techniques have become increasingly important in the field of structural dynamics, as they offer advantages over contact techniques by overcoming their limitations. These limitations include the effect of added masses and the challenges associated with data transmission in rotating machinery. Among non-contact techniques, Laser Doppler Vibrometers (LDVs) are distinguished by their outstanding qualities of high sensitivity, high accuracy and high acquisition speed [1]. However, single point measurements may not be suitable for describing complex deformed shapes. Therefore, more sophisticated measurement configurations are commonly used. In [2] an LDV sensor was mounted on a robotic arm to speed up the acquisition process, while in [3] a Scanning LDV (SLDV) was used to increase the number of measurement points. Although these approaches have proven effective, they cannot be classified as full-field methods. This is because the use of a single vibrometer limits measurements to only one dimension (along the beam axis), imposes limitations on the number of measurement points, and prevents simultaneous measurements at different points.

For these reasons, extensive research efforts have been devoted to the advancement of full-field 3D measurement techniques. Although Digital Image Correlation (DIC) was originally developed for static acquisitions, the development of high-speed cameras has opened up the application of the method to vibration measurements. The work reported in [4] discusses the advantages and limitations of using DIC for experimental modal analysis compared to impact hammer and Scanning Laser Vibrometry (SLV). This study demonstrates that DIC, using two high-speed cameras, is effective in analyzing the deformed shapes of a dryer-cabinet panel. In [5] it has been proven that updating the localized parameter model performed with full-field measurements (cameras) is more

accurate and efficient than that performed with single-point measurements (accelerometers). In [6], the 3D-DIC technique was compared to a 3D scanning LDV system for analyzing the dynamics of a metal plate. The study showed that while SLDV required a long time to scan the sample, the simultaneous sampling of multiple points with the DIC technique significantly shortened the acquisition time. Additionally, although the noise floor for SLDV is significantly better than DIC for out-of-plane measurements, they are approximately equal for in-plane results. This, combined with the lower costs of DIC setups, makes 3D-DIC a good solution for three-dimensional surface motion measurements. In [7], 3D-DIC experimental modal analysis was performed on a large metal panel. To improve the signal-to-noise ratio and enhance DIC accuracy, the recorded motion captured by high-speed cameras was magnified using a phase-based motion technique. The importance of full-field measurements can be further emphasized when nonlinear phenomena are to be studied, as they enable the acquisition of detailed information on the spatial distribution of deformations, facilitating a better understanding of the complex behavior exhibited by nonlinear systems. Nonlinear phenomena commonly occur in structures that have contact surfaces. For example, in the case of turbine such contacts occur at the blade root or under the blade platform [8], where friction dampers are implemented to mitigate the vibration amplitude. Accurate measurement of the relative displacement between contact surfaces is critical in addressing contact problems, as it allows for a better understanding and more effective management of them. A number of papers in the literature deal with the measurement of nonlinear phenomena using DIC techniques. A combined high-speed camera and DIC analysis was applied in [9] to gain an in-depth understanding of the global and local motion of an underplatform damper. Nonlinear vibro-impact phenomena were analyzed in [10] to estimate the Coefficient Of Restitution (COR) and friction forces, which were used to implement different contact models. The nonlinear vibrations of a saxophone reed was studied in [11] by using the stroboscopic effect. The strobe light allowed the amplitudes of different harmonics to be evaluated while the reed was subjected to purely sinusoidal excitation. In [12] DIC technique and a high-speed camera were used to make measurements of the waves propagating along a thin plate floating on the surface of the water, revealing non-linear components that introduce asymmetries in the wave shape. In [13] a comparison was made between SLDV and DIC, with high speed cameras, in measuring the linear and nonlinear response of a nominally flat beam and plate under a sinusoidal load in steady state. The beam and plate were clamped-clamped and nonlinearities were triggered by large deflections. Small displacement amplitudes are often difficult to measure because of the noise that typically affects high-speed cameras. The work presented in [14] addresses this problem and shows that by using the Least-Squares Complex-Frequency method combined with the Least-Squares Frequency-Domain method, modal identification is still possible. DIC was used in [15] was used to visualize the local kinematic behaviors of a jointed interface. Slip and separation was measured with high resolution at the interface of a bolted joint. The full-field nonlinear dynamics was measured using high frame-rate cameras on a jointed structure in [16]. Because high-speed camera fan noise is injected into the measurements, the accuracy of the DIC was validated using accelerometer data. The follow-up paper [17] exploit the use of high spatial resolution data to compare different nonlinear system identification methods. The paper presented in [18] develops a novel modal decomposition method, called smooth mode decomposition (SMD), to manage the excessive storage and computational requirements and the temporal aliasing effect associated to full-field sensory techniques. This method was applied to a set of full-field displacement data obtained from the 3D digital image correlation (DIC) to validate the capability of the proposed SMD in identifying linear normal modes from full-field measurements.

All these approaches have provided promising results in applying full-field DIC measurements to nonlinear phenomena by exploiting high-speed cameras. However, higher frame rates can be achieved only by reducing the image resolution, which results in sensitivity loss for small displacements. Moreover, the high cost of high-speed cameras makes them unaffordable for most research centers. Accordingly, several approaches have also been developed in the literature to use high-resolution, low-speed cameras to measure high-frequency linear vibrations. The challenge is to overcome the Nyquist–Shannon theorem. In [19] the downsampling approach was applied to band-limited signals. In [20], low-speed cameras and the DIC technique were used to analyze the deformed shapes of a rotating disk by employing stroboscopic lights and a downsampling technique. Nevertheless, the feasibility of these approaches in the case of nonlinear phenomena has not yet been investigated. The first attempt to nonlinear modal analysis using low-frame cameras was done in [21]. A different approach was proposed in [22] where images captured by the cameras were synchronized exploiting the signal of an LVD with high frequency resolution.

1.2. Objective

The objective of this work is to develop a methodology for using standard high-resolution, low-speed cameras to study nonlinear phenomena at high-frequency. This is made possible with an algorithm that correctly reconstructs a downsampled signal avoiding aliasing error. Accordingly, a new downsampling method, denoted *Smoothed Harmonics Analysis* (SHA), was developed and applied to reconstruct the response of a beam with step wise boundary conditions that trigger nonlinear behavior. This paper is organized as follows. Section 2 briefly summarizes the basic procedure for measuring displacements of a structure using cameras whose frame rate is less than the vibration frequency and Nyquist's condition is not satisfied. This Section is introductory to the problem and can be skipped by the reader familiar with DIC along with a downsampling procedure. Section 3 explains the detail of the method proposed to reconstruct a multi-harmonic signal with downsampled data. The test case is described in Section 4. This Section describes both the experimental set up and a semi-analytical solution found in the literature. The semi-analytical solution helps to find the right choice for the approximation of the target solution. The simulation results are shown in Section 5. One point was used as reference point to evaluate the reliability of the method: the displacement of this reference point was measured with an LDV sensor and compared with the displacement determined by the proposed method.

Notation and convention: Throughout this paper vectors and matrices are denoted by boldface letters. If not explicitly stated otherwise vectors are column vectors. The symbol $^\top$ indicates the transpose of a vector or matrix.

2. Measurement process

The measurement process in which DIC is applied to downsampled signals is summarized as follows.

- Specimen preparation: DIC analysis requires uniqueness in the image of the set of pixels (subsets) representing a point on the surface of the specimen. Consequently, when the surface does not naturally fulfill this requirement, proper preparation becomes fundamental. Typically, a speckle pattern is employed to ensure accurate and precise DIC measurements. In [23], various pattern generation techniques are examined, taking into account the vast diversity in test materials, spatial scales, and experimental conditions.
- Image acquisition at a frame rate lower than the Nyquist sampling rate (downsampling): valuable guidance on setting environmental and camera parameters to capture high-quality images of a moving object can be found in the literature. In particular, clear and concise guidelines on general camera settings are provided in [24]. The setting of sampling parameters (frame rate and recording time) is discussed in Section 3.
- Image processing by DIC algorithm: it enables the calculation of the displacement field of the specimen for each frame. The fundamentals of this process are illustrated in Section 2.1.
- Signal reconstruction of downsampled signals at each DIC point: it allows to accurately estimate the displacement field over time, avoiding aliasing errors. Brief descriptions of downsampling algorithms are provided in Section 2.2, whereas the Smoothed Harmonic Analysis algorithm, employed in this paper, is presented in Section 3.

2.1. Digital image correlation

There are three fundamental steps typical of stereo-DIC algorithms: system calibration, processing two sets of images acquired from two different perspectives using 2D-DIC algorithms, and triangulating the 2D position of each point tracked by the cameras. For each camera in a stereo pair, calibration aims to determine both intrinsic parameters, which define the geometric and optical characteristics of the camera, and extrinsic parameters, which define the position and orientation of the camera relative to a global coordinate system. Intrinsic and extrinsic parameters describe the transformation that maps each image point on the camera sensor to its corresponding 3D point in the global coordinate system according to the pinhole optical model [25]. In this work, open source codes were used to perform 3D-DIC analysis. The first step was addressed by using the MATLAB Stereo Camera Calibrator App [26]. Then, the obtained stereo-parameters were used to triangulate at each frame the image points computed by the open source 2D-DIC software Ncorr [27]. Ncorr is a subset-based DIC algorithm. In this method, each measurement point is represented by a circular group of pixels known as subsets, defined in the reference image. To do that users can specify the subset size (radius of each circle in pixels) and grid spacing (distance in pixels between contiguous subset centers). The algorithm tracks the shape and position of reference subsets across deformed images (deformed subsets). To determine the deformation of a subset, DIC algorithms search for the extremum of a correlation function. This process involves an iterative process where deformation is assumed to be homogeneous within each subset and the transformation between the reference and deformed subsets is defined by shape functions. In Ncorr the transformation is constrained to a linear first-order deformation, allowing translation, shear and normal deformation of subsets.

2.2. Downsampling methods

The Nyquist–Shannon theorem establishes that in order to accurately sample a periodic signal, the sampling rate must exceed twice the frequency of the highest component of interest in the signal. However, in situations where it is not feasible to meet the requirements of the Nyquist theorem because the frequencies involved are much higher than the maximum sampling rate of the measuring instrument, it becomes necessary to employ downsampling and signal reconstruction techniques. These approaches prevent loss of information and aliasing error, where high-frequency components appear as lower-frequency ones, distorting the original signal and introducing unwanted artifacts. Recent research shows that it is possible to reconstruct a downsampled linear and stationary response to a single harmonic excitation. In particular, in [28] Non-Harmonic Fourier Analysis (NHFA) has been implemented. NHFA mainly consists in correctly reconstructing a signal by finding the best-fit, with a single harmonic at the same frequency as the excitation, of the downsampled signal. Another technique [29] consists in extending the acquisition time over several periods by setting a sampling period T_s larger than an integer multiple of the period of vibration T_v, i.e. $T_s = k\,T_v + \Delta t$. This procedure is depicted in Fig. 1, where the parameter k was set to two, which means recording one sample every two periods. Thus, through a back-translation of the samples taken at different periods, the signal is effectively sampled within a single period at a fictitious frequency that is higher than the actual frequency of the measuring instrument. In Fig. 1 a sinusoidal signal with a frequency of 1 Hz was sampled at 0.47 Hz, thus at a sampling rate lower than its Nyquist frequency, resulting in a signal affected by aliasing. After back-translation of the measured points, it is possible to fictitiously sample a period of the signal at a frequency of 7.5 Hz, which is higher than the Nyquist frequency.
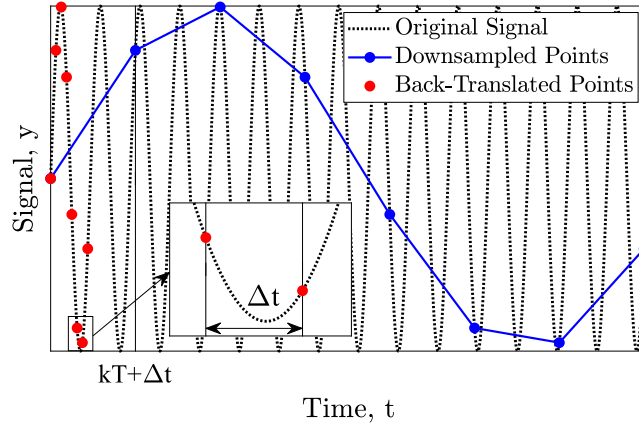
Fig. 1. A generic signal y sampled with a sampling rate lower than its Nyquist frequency and its recovery by back-translation.

3. Smoothed harmonics analysis

It is well known that a periodic signal, denoted as y, can be represented as a combination of sine and cosine using the Fourier series.

$$y(t) = \sum_{j=0}^{\infty} \left(A_j \cos \left(\omega_j t \right) + B_j \sin \left(\omega_j t \right) \right) \tag{1}$$

where ω_j is the jth harmonic frequency and A_j and B_j are the amplitudes of cosine and sine, respectively. From a practical point of view, all experimental signals are discrete and finite, because they consist of a finite number of samples recorded at different instants within a finite time interval. However, it is still feasible to analyze the harmonic components of such signals using a Discrete Fourier Transform (DFT) and approximate the signal with a finite number of harmonics. This approach has limitations, as the frequency resolution depends on the sample length and thus may not be able to accurately calculate every harmonic in the signal. In addition, if a downsampled signal is analyzed with DFT, the resulting frequency content detection will be incorrect (aliasing). Both the Smoothed Harmonics Analysis (SHA), which is presented in this paper, and the Non-Harmonic Fourier Analysis (NHFA) offer effective approaches to accurately reconstruct a downsampled signal that has a limited number of significant harmonics. Both methods assume that the frequencies of the harmonics are known. This requirement may limits their applicability, making them unsuitable for test cases where the frequency composition of the sampled signal is unknown. This is the case, for example, with nonlinear structures, whose response to even a controlled single harmonic excitation can be unpredictable. However, for the purposes of this study, this limitation can generally be overcome. In fact, low-frame rate cameras capturing the full-field system dynamics can be paired with a single-point, high-frame-rate device (such as microphone, accelerometer, vibrometer, etc.) to detect the primary harmonics of the structural response. These detected harmonics can then be utilized for accurately downsampling and reconstructing DIC measurements. Thus, these methods determine the amplitude and phase of each harmonic by finding the best-fit to the acquired samples. Specifically, the NHFA method is an iterative process in which a harmonic contribution is detected and removed from the downsampled signal at each iteration. The SHA method, on the other hand, calculates all harmonic contributions simultaneously. As a result, these two algorithms exhibit different features when applied to a generic downsampled signal. The different behavior of the two methods is compared in Section 3.1. The SHA method is described in detail below.

Eq. (1) written in matrix form gives

$$y(t) \approx (1 \ \dots \ \cos(\omega_j t) \ \sin(\omega_j t) \ \dots \ \cos(\omega_m) \ \sin(\omega_m t)) \begin{pmatrix} A_0 \\ \vdots \\ A_j \\ B_j \\ \vdots \\ A_m \\ B_m \end{pmatrix} \tag{2}$$

where ω_j is the jth frequency component of the signal, A_j and B_j the amplitude of the corresponding harmonics and m is the total number of harmonics. In short form Eq. (2) becomes

$$y(t) \approx \mathbf{p}^{\mathsf{T}} \cdot \mathbf{q} \tag{3}$$

where the harmonics used to approximate the signal were placed into vector $\mathbf{p}$ while $\mathbf{q}$ contains the amplitude of each harmonic.

If **p** and n discrete values of y are known at different instants of time t_i, it is possible to compute the amplitudes in **q** by finding the best-fit of the n samples from the m harmonics. The best-fit can be found by minimizing the objective function

$$\Theta = \frac{1}{n} \sum_{i=1}^{n} \left(y_{t_i} - y_{t_i}^e \right)^2 = \frac{1}{n} \sum_{i=1}^{n} \left(\mathbf{p}_{t_i}^T \cdot \mathbf{q} - y_{t_i}^e \right)^2 \tag{4}$$

where $y_{t_i}^e$ is the ith experimental sample. In this paper y is the response of a mechanical system, in terms of displacements, excited by external forces. Minimizing the objective function with respect to **q** means setting the first derivative of the objective function equal to zero [30]

$$\frac{d\Theta}{d\mathbf{q}} = \mathbf{A}\mathbf{q} - \mathbf{b} = 0 \tag{5}$$

In Eq. (5) **A** and **q** are the $(2m+1) \times (2m+1)$ matrix and the $(2m+1)$ vector

$$\mathbf{A} = \frac{1}{n} \sum_{i=1}^{n} \mathbf{p}_{t_i} \cdot \mathbf{p}_{t_i}^T$$
$$\mathbf{b} = \frac{1}{n} \sum_{i=1}^{n} \mathbf{p}_{t_i} \cdot y_{t_i}^e \tag{6}$$

The best-fit vector $\mathbf{q}^s$, computed by solving Eq. (5) as a function of the unknown **q**, gives the amplitude of each harmonic that has been kept in the response. The approximated response, reconstructed from the under-sampled signal according to Eq. (3), is then

$$y(t) \approx \mathbf{p}_{(t)} \cdot \mathbf{q}^s \tag{7}$$

Therefore, this method makes it possible to reconstruct the downsampled signal while avoiding aliasing if the frequency values of the main harmonics are assumed to be known.

To ensure the effectiveness of the algorithm, it is essential that the sampling period T_s is not an integer multiple n of the signal fundamental period T_v, which is here defined as the least common multiple of the periods of the frequencies that compose the signal,

$$T_s \neq nT_v \tag{8}$$

If this condition is not met, the same signal point will be sampled at different intervals, resulting in redundancy of information within the period and, consequently, poor information for the algorithm. Conditions in Eq. (8) can be fulfilled by several sampling frequencies. A relationship between the number of samples to be acquired, denoted as n_s, at the sampling rate f_s can be written as

$$f_s = \frac{1}{T_s} = \frac{1}{kT_v + \Delta t} \tag{9a}$$
$$n_s = \frac{T_v}{\Delta t} \tag{9b}$$

where k and Δt are parameters that must be set as a function of the maximum speed of the measurement device and of the highest frequency of the signal. The meaning of these parameters is illustrated in Fig. 1. In particular, Δt must be set small enough to correctly describe the highest harmonic component of the signal, and k must be chosen high enough so that the sampling rate falls within the range of the measuring instrument. Sampling parameters set according to (9) provide a dense description of the period (fictitiously sampled at a resolution of Δt) and minimize the total acquisition time.

3.1. Sensitivity to noise and sampling parameters

This section presents the results of numerical testing to illustrate the performance of the proposed SHA method. Subsequently, the results were compared with those obtained using the previously mentioned NHFA method. The algorithm's behavior was tested with varying downsampling parameters, namely the number of acquired samples and the sampling frequency. Given the possibility of neglecting some harmonics of an under-sampled signal in real scenarios, it is also useful to investigate its impact on the detected amplitudes of harmonics. Therefore, the algorithm was tested by calculating the amplitude of a single harmonic within a multiharmonic signal. The test involves progressively increasing the number of harmonics considered, starting from one (in which only the target harmonic was considered) up to considering all harmonics.

For this purpose, a test signal was generated with 5 harmonics, whose amplitudes are given as reference amplitudes. The fundamental period, that is the lowest common multiple of the periods of the five harmonics, is 0.01 s and the maximum frequency is 1 kHz. White noise, with a signal-to-noise ratio of 10 dB, was also added to the signal to simulate the perturbation on measured signals. The test signal is shown in Fig. 2a, together with the aliased signal obtained with a sampling frequency of 39.84 Hz, chosen as suggested by Eq. (9a) with $k = 2.5$ and $\Delta t = 10^{-4}$ s. The SHA algorithm was applied to the aliased signal resulting in the signal plotted in blue in Fig. 2b. The figure compares the recovered signal to the original test signal, with (in blue) and without (in red) noise. In the absence of noise, the difference between the recovered and the original test signal is negligible, whereas, in the presence of noise, the recovered signal can no longer follow the higher frequency introduced by the noise.

In addition, to evaluate the algorithm's ability to detect amplitudes of each wave when the series is truncated, the aliased signal was recovered by progressively increasing the number of harmonics in Eq. (2). The amplitude of the first harmonic as a function of
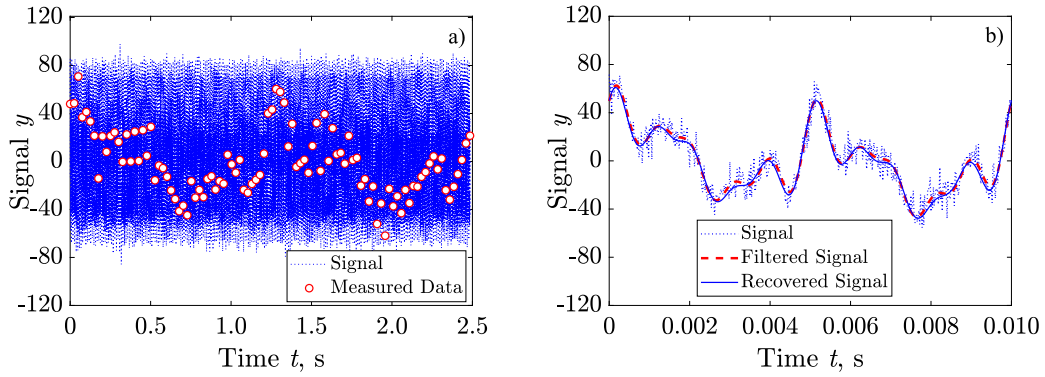
Fig. 2. Figure (a) shows a periodic y-signal created as a sum of five harmonics and white noise; aliased data resulting from its downsampling are also shown. Figure (b) displays a period of the y-signal resulting from aliased data recovery by the SHA method. It is superimposed on the original signal and the filtered signal.
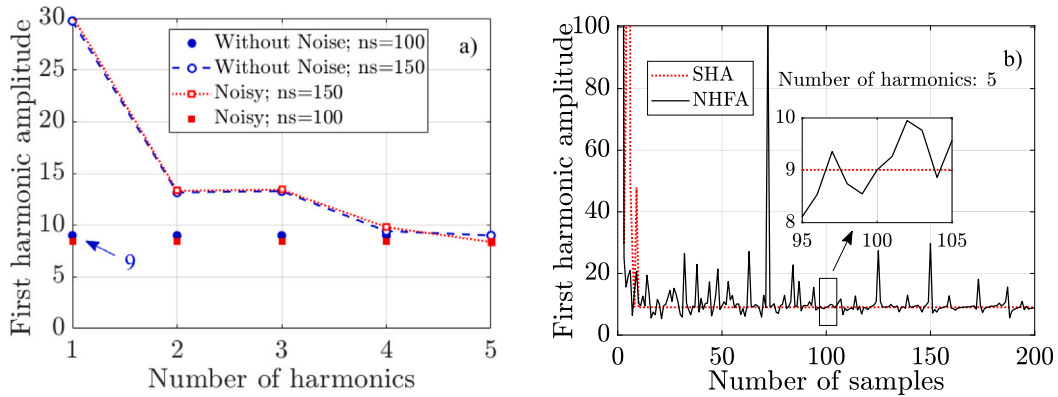

Fig. 3. (a) Amplitude of the first harmonic calculated by the SHA as a function of the number of harmonic contributions considered by the method; (b) Amplitude of the first harmonic computed by SHA and NHFA as a function of the number of samples of the downsampled signal.

the number of harmonics is shown in Fig. 3a. If the number of samples of the downsampled signal is chosen according to Eq. (9b), n_s = 100 in the example shown in Fig. 2, the amplitude of the harmonic calculated by the SHA method is independent of the number of harmonics used to recover the signal. On the other end, if n_s does not comply with Eq. (9b) (n_s = 150 in the example) the amplitude varies with the number of harmonics approaching the reference value if the samples are not affected by noise.

Although obtained empirically, this result leads to two considerations. First, when the harmonic series is truncated, the downsampled signal is more accurately recovered if the sampling parameters are set according to Eq. (9). Second, even in case of random downsampling, the SHA method provides the exact result if all harmonics of the test signal are considered. This is an advantage over the NHFA method, in which the contribution of each harmonic is calculated separately. This feature is highlighted in Fig. 3b, which shows the amplitude of the first harmonic as a function of the number of samples. Calculations were performed by SHA and NHFA methods, considering all harmonics of the signal and fixing the sample length. The two methods give the same result only if the aliased signal is described by an integer multiple of n_s determined according to Eq. (9b), while for different n_s the result of the SHA method is more accurate.

4. Test case

Before starting the experimental campaign, several nonlinear systems were simulated in search of a system capable of triggering nonnegligible nonlinearities in order to validate the performance of the proposed method. Among these systems, the impact of a light beam on an obstacle showed the greatest harmonic distortion. Therefore, the test case chosen as the benchmark is the forced-response of a beam with step wise boundary conditions. One end of the beam is clamped on the moving coil of an electromagnetic shaker. The other end is free to move in one direction but impacts a rigid obstacle in the other direction, as shown in Fig. 4. This step wise boundary conditions triggers a nonlinear behavior of the motion of the beam. The beam, made of aluminum, is 280 mm long, and has a cross-section of 25 × 5 mm. The motion of the beam was tracked by utilizing a low-frequency stereo-camera system and DIC technique. The aliased displacement map was then recovered by the SHA method.
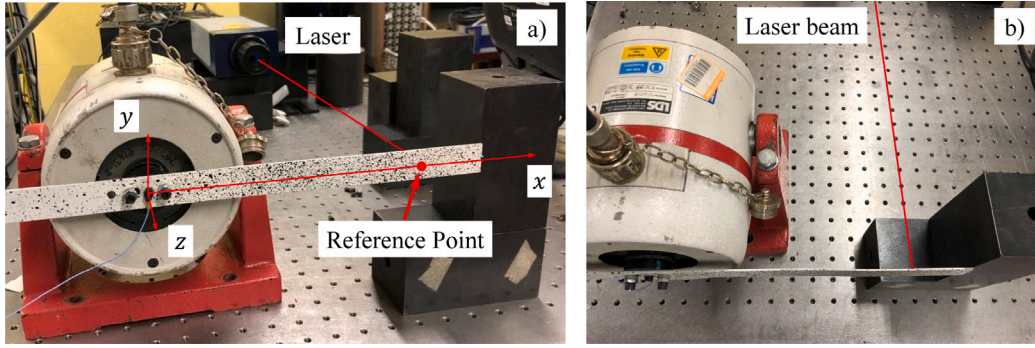
Fig. 4. Experimental setup: beam clamped to a shaker and impacting a rigid obstacle during motion: (a) front view and (b) top view.

Because of the nonlinear behavior, the motion of the beam contains superharmonics of the excitation frequency but also subharmonics, as predicted in [31]. This behavior has been accurately measured with a high-resolution, high-frequency laser vibrometer (LDV) on a reference point of the beam. Section 4.1 provides a brief numerical analysis of the nonlinear behavior exhibited by the system. The experimental setup and corresponding results are then presented in Section 4.2.

4.1. Test planning

A semi-analytical solution of the test case, a beam impacting on a obstacle, was provided in [32,33]. Since the beam was excited at a frequency close to its first resonance, the beam response w – function of the axial coordinate x and time t – was approximated by considering both the first modal shape of the cantilever beam $\psi_1(x)$ and of the clamped-supported beam $\psi_2(x)$, as illustrated in Fig. 5. Therefore, it is possible to describe the bending displacement v of the beam as a function of $\psi_1(x)$ and $\psi_2(x)$ and their respective modal amplitudes $a_1(t)$ and $a_2(t)$, as

$$\begin{cases} w_1(x,t) = a_1(t)\psi_1(x) & a_1 < 0 \\ w_2(x,t) = a_2(t)\psi_2(x) & a_2 > 0 \end{cases} \tag{10}$$

The equation of motion of a beam clamped to a moving support is

$$D\frac{d^4w}{dx^4} = -m\left(\frac{d^2w}{dt^2} + \frac{d^2W}{dt^2}\right) \tag{11}$$

where D is the bending stiffness of the beam, m the mass per unit length and $W(t) = W_o cos(\omega t)$ the harmonic displacement imposed to its clamped end. Substituting Eq. (10) into Eq. (11) yields the equations of motion of the system, which are solved in the time domain by Runge–Kutta integration. Fig. 6 shows the result of the displacement of a point at the center of the beam, i.e. for $x = L/2$ as defined in Fig. 5, in the time and frequency domain. Simulations were performed with amplitude $W_0 = 10$ mm and frequency $\omega = 130.9$ rad/s (20.8 Hz), corresponding to the first resonance frequency of the clamped-free beam. The model predicts the sub-harmonic and super-harmonic frequencies of the excitation in the response spectrum. Therefore, the results of this simplified model were used to guide the SHA method in recovering the displacement from the downsampled signals measured by the cameras. Specifically, the steady-state response from the semi-analytical model was downsampled and reconstructed using an increasing number of harmonic contributions to determine the optimal number of harmonics required for accurate signal reconstruction. For this purpose, 180 samples (blue dots in Fig. 7a) were extracted from the original signal (represented by the blue line) and were processed by SHA. These samples were selected according to Eq. (9), by choosing $k = 0.5$ and $\Delta t = 0.053$ µs, resulting in a sampling frequency f_s of 20.6 Hz. The cross-correlation coefficient C is used to evaluate the similarity between the original and reconstructed signals. If w_1 represents the original signal and w_2 the reconstructed one, sampled with N samples, it is defined as:

$$C(w_1, w_2) = \frac{1}{N-1}\sum_{i=1}^{N}\left(\frac{w_{1,i} - \mu_1}{\sigma_1}\right)\left(\frac{w_{2,i} - \mu_2}{\sigma_2}\right), \tag{12}$$

where μ and σ are the mean and standard deviation of the signals. The cross-correlation coefficient is plotted in Fig. 7b as a function of the number of harmonics input to SHA. The correlation coefficient is lower than 0.8 when only the first harmonic (the subharmonic) and the second one (at the excitation frequency) are considered, and it asymptotically approaches 1 as the number of harmonics increases. According to these results, 12 harmonics, which yield a correlation coefficient of 99.98%, were considered for reconstructing the signal. The reconstructed signal is shown in red in Fig. 7a.

4.2. Experimental setup

Fig. 4 shows the experimental setup, namely a beam clamped to the moving coil of a shaker with the free end impacting on a rigid obstacle. A speckle pattern was sprayed to the surface of the beam to properly perform the DIC analysis. The scale of images used
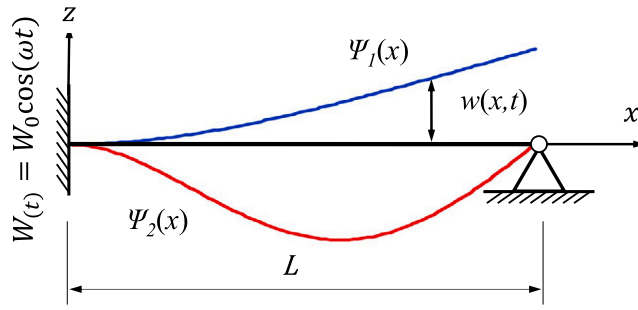
Fig. 5. Sketch of the experimental setup. The two modal shapes, $\psi_1(x)$ and $\psi_2(x)$, used in the simulation are displayed.
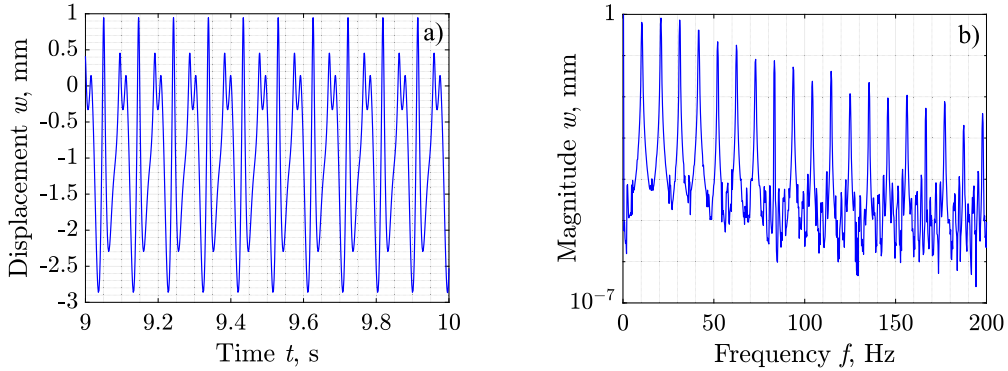

Fig. 6. Time history (a) and spectrum (b) of the flexural steady state displacement $w(z, t)$ of the middle point ($x = 140$ mm) of the beam resulting from the analytic model.
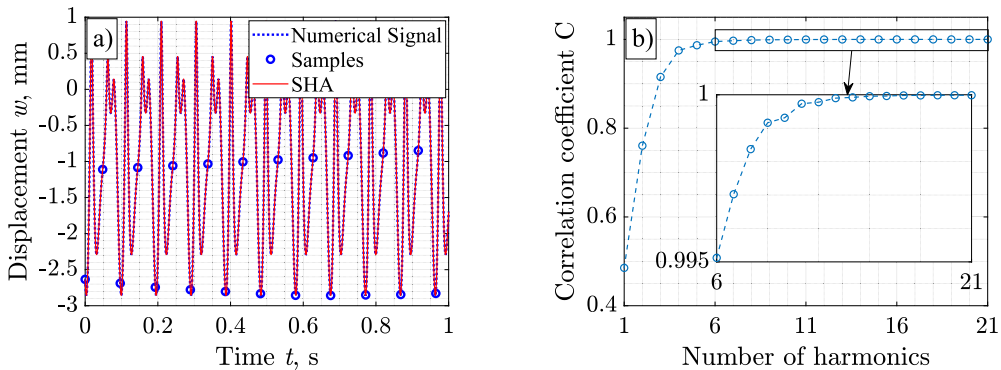

Fig. 7. (a) Steady-state response resulting from the semi-analytical model (blue dotted line) and its downsampled samples (blue dots). The reconstructed signal from the downsampled one using the SHA with 12 harmonics is shown with a red line. (b) Cross-correlation coefficient between the numerical and reconstructed response as a function of the number of harmonics contributions considered by the SHA algorithm.

for DIC analysis is around 80 μm/pixel, resulting in a sensitivity of the DIC system of about 10 μm. The excitation was obtained by a signal generator, which was used to create a monotone harmonic signal at 24 Hz, specifically chosen to be near the first resonance frequency of the clamped-free beam. The Digital Image Correlation (DIC) hardware consists of two Optomotive Spinosours cameras, each equipped with a 23 MP Fujinon lens with a 35 mm focal length. These cameras are equipped with a high-resolution sensor capable of recording 7.1 MP images at their maximum frame rate (200 fps). In this work, images were acquired at a frame rate of 23.7 fps, lower than the maximum allowed and according to Eq. (9). The shutter time plays a crucial role in dynamic acquisition, as a short shutter time is essential to freeze the scene and to prevent capturing blurred images. Selected cameras are characterized by a minimum shutter time of 2 μs that makes them suitable for this test. Thus, high-intensity external light is needed to compensate for the loss of image brightness caused by a shorter shutter speed and the resulting underexposure. Therefore, two 200 W Stratus LED modules equipped with parabolic reflectors were introduced to illuminate the scene. The captured images were stored in a dedicated computer connected to the cameras.
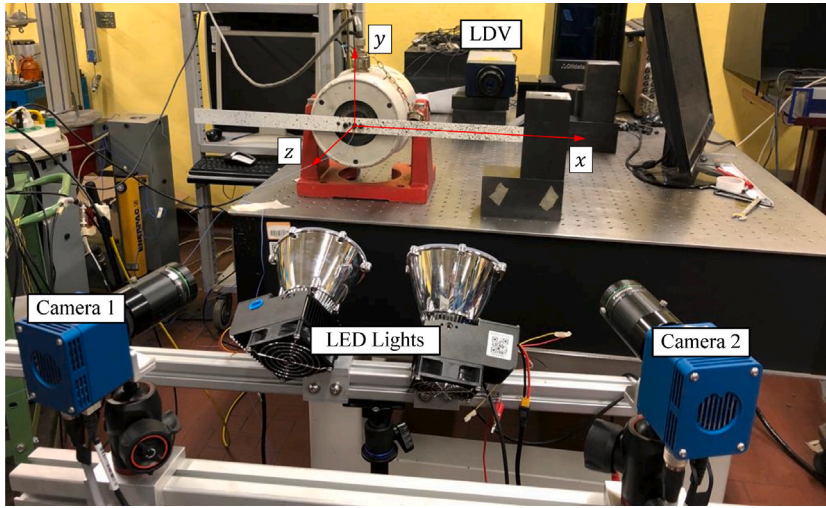
Fig. 8. Experimental setup: the motion of the front side of the beam is captured by the stereo-camera system, while the motion of a reference point in the rear part of the beam is measured using a LDV.
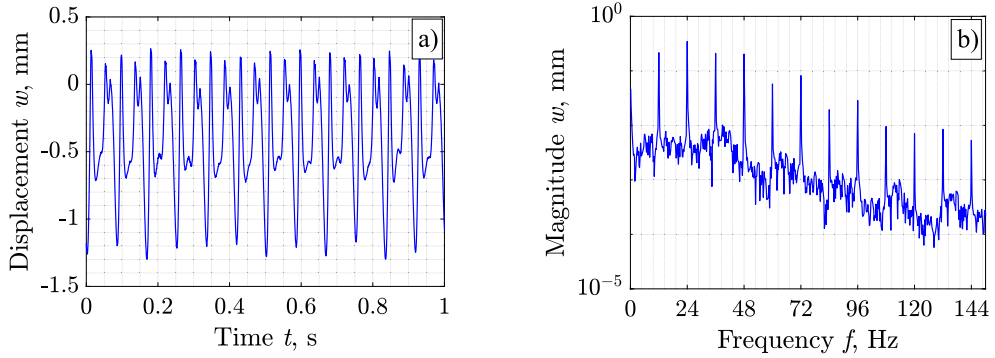

Fig. 9. Displacement w determined by the velocity measured with the LDV at the reference point, on the centerline of the beam and 50 mm from the tip, in the time domain (a) and in the frequency domain (b).

The motion, in terms of velocity, of a reference point was measured also with a high-resolution Laser Doppler Vibrometer (LDV) and then integrated to obtain its displacement. The initial condition $w(0)$ for the integration is unknown as the LDV data were recorded from a time other than $t = 0$. In contrast, DIC measures displacements using a reference image of the structure taken at rest, when all displacements are zero, $w(0) = 0$. Integration was then performed using as initial condition the displacement measured with the DIC. The LDV was placed behind the beam, as shown in Fig. 8 and the out-of-plane (along the z-direction) displacement w was measured with high accuracy (0.1 μm) and high sampling frequency (50 kHz).

5. Results

The displacements w of the reference point measured with the LDV were compared with the displacements measured with the proposed method. In addition, the reference point displacements were also used to detect superharmonics and subharmonics resulting from nonlinearity. The displacement w of the reference point is shown in Fig. 9a while its spectrum is presented in Fig. 9b.

The spectrum clearly shows the presence of superharmonics as multiple of the excitation frequency $f_0 = 24$ Hz. Moreover, also a subharmonic is present, whose frequency is half the excitation frequency $f_{sub} = 24/2$ Hz, with its multiple $n f_{sub}$. The spectrum of laser response indicates that the relevant frequencies are in the range 12–144 Hz and confirms the harmonic content predicted by the theoretical analysis. This observation will guide the application of the SHA method. Cameras were set to capture 180 frames at 23.7 fps, as suggested by Eq. (9) with $k = 0.5$ and $\Delta t = 0.046$ μs. Fig. 10 illustrates the downsampled signal of the displacement w at the reference point measured by DIC (blue dots) and the corresponding signal recovered by the SHA (red line). The signal was recovered using the subharmonic f_{sub} and the first 11 multiples in the Fourier series of Eq. (3).

Fig. 11 compares the displacement w at the reference point recovered with DIC and the SHA method and the LDV measurement. The cross-correlation coefficient, defined in Eq. (12), is equal to 99.3%. Thus, the two measurements are in good agreement. The
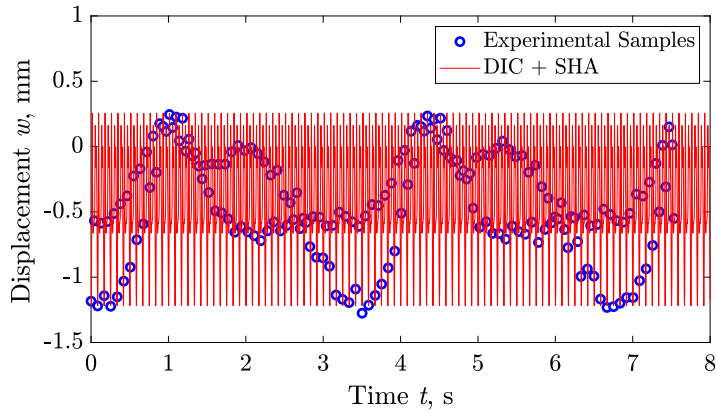
Fig. 10. Downsampled data at the reference point (experimental samples from DIC) and the displacements w as recovered with SHA.
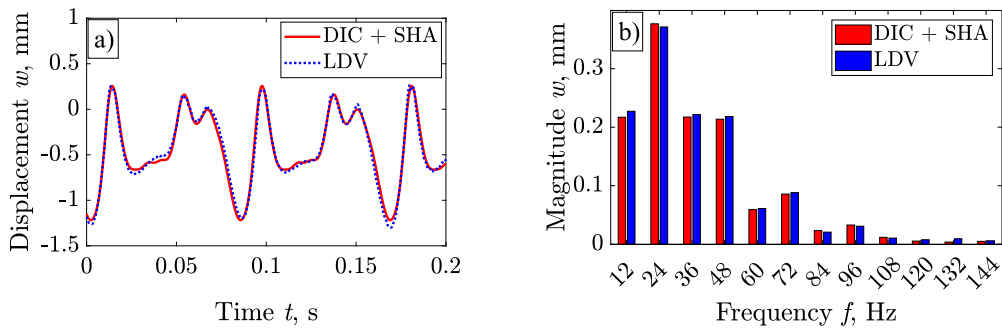

Fig. 11. Comparison of displacements measured at the reference point by a low frame-rate DIC with the LDV; Figure (a) shows the superposition of the two signals in the time domain while Figure (b) depicts the histogram of the amplitudes of the first harmonics in the frequency domain.

differences are of the same order as the accuracy of the DIC measurement device. In addition, both laser and camera measurements experience inevitable misalignments and disturbances, so the mismatch between the results seems reasonable.

As a further checking, the aliased samples were back-translated into a single period $T_{sub} = 1/f_{sub}$ associated to the 24-Hz subharmonic and processed with DFT. The result obtained on the reference point is shown in Fig. 12 together with the harmonic content achieved with SHA and the spectrum of LDV on the same point. The results of the two downsampling methods are in good agreement and the small discrepancy between the calculated spectra can be explained by the low resolution of the spectrum calculated by the DFT. However, the application of the DFT method yields a cross-correlation coefficient of 97.2% between the reconstructed and the LDV signals, which is lower than the one computed by the SHA. Indeed, the main limitation of the DFT approach comes from its frequency resolution [34,35], which varies with sample number. It means that frequency components of the signal that are not integer multiples of the reciprocal of the acquisition period cannot be accurately detected by DFT.

The full-field dynamics of the beam is achieved by recovering the displacements at all the DIC measurement points. Fig. 13 shows the displacements w at three different points along the beam: near the free end, where the beam impact the obstacle, at an intermediate point, and near the clamped end of the beam. In the same figure, eight significant instants of time are labeled with the letters A through H, while the deformed shapes at the same instants are shown in Fig. 14 and labeled with the same letters. The displacement was amplified by a factor of 100 to highlight the deformed shapes; the actual value of the displacement is represented by the color scale on the right side. The black cylinder visible in the images represents the estimated location of the obstacle.

6. Conclusion

This paper has presented a novel methodology to extend the applicability of the DIC technique to the study of the dynamic response of nonlinear systems under the assumption of periodic and steady-state vibrations. The method has been developed for cameras with low frame-rate that does not allow the Nyquist–Shannon theorem to be satisfied. Thus, this methodology allows for high-resolution analysis of high-frequency dynamics, overcoming the limitations of high-speed cameras, which are characterized by relatively low resolution and high cost. This is the first time that low frame-rate DIC has been applied to the dynamic analysis of nonlinear structures, thus advancing this field of research. At the heart of the method is a new algorithm called Smoothed Harmonic Analysis (SHA). Comparison of SHA with other well-known spectral analysis methods (DFT and NHFA) suggests its potential for
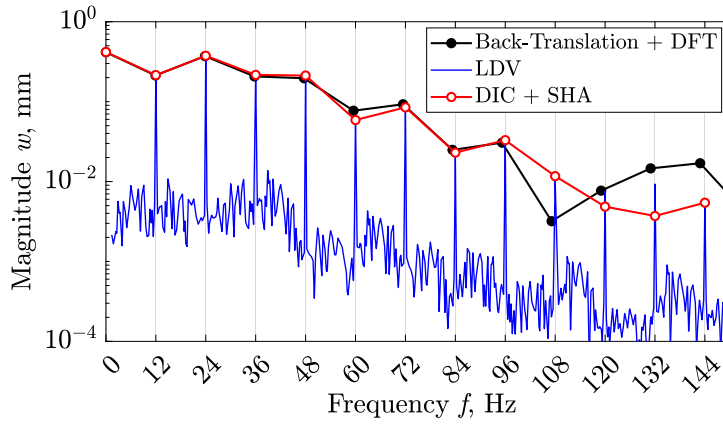
Fig. 12. Comparison of spectra computed for downsampled signal recovering: in black the spectrum computed by the Discrete Fourier Transform (DFT) of the signal obtained moving the samples computed by DIC in the first period of vibration of the beam and in orange the spectrum reconstructed by the SHA method. The blue spectrum illustrates the DFT of the laser signal.
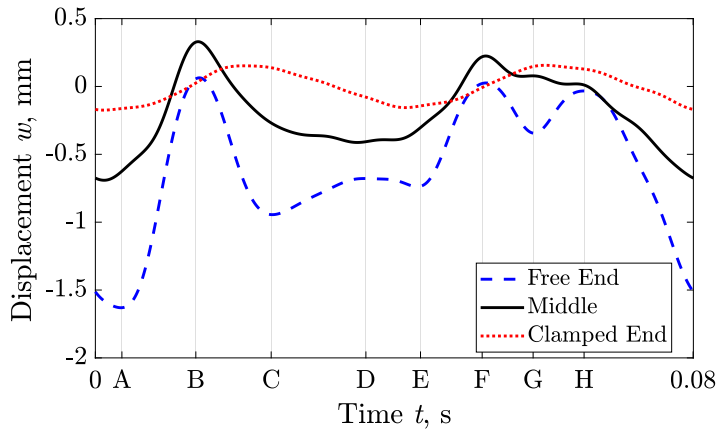

Fig. 13. Out-of-plane displacement w computed by DIC and SHA methods at three points along the beam: the blue, black, and red lines represent displacement signals extracted at a point near the free end, at a midpoint, and near the clamped end of the beam, respectively. Letters from A to H label times at which there is a change in the sign of the velocity of some points on the beam.

accurate and efficient spectral analysis of a downsampled signal characterized by multiple harmonic components whose frequencies are supposed to be known. The performance of the method has been tested both numerically and experimentally.

To demonstrate its feasibility the methodology was applied to the analysis of the nonlinear response of a beam with one clamped end and a step wise boundary condition at the other end. The beam was excited by a 24-Hz single harmonic force while the response, in terms of images, was recorded with cameras at a sampling rate 23.7 fps in the range 10–150 Hz. Due to the nonlinear nature of the system, the response contains superharmonic and subharmonic of the excitation frequency. Consequently, the chosen sampling rate does not meet the requirements of the Nyquist theorem, making the DIC technique alone unsuitable for accurately capturing the system dynamics. A qualitative numerical model was used to predict the frequency content of motion that was then confirmed by measurements made with high-resolution, high-speed LDV. The test results demonstrate that by computing the signal as a function of time, the SHA method decouples the signal reconstruction process from the acquired samples. This decoupling is critical to avoid aliasing errors when reconstructing a downsampled periodic response acquired by cameras, since it allows the choice of the temporal discretization of the response, ensuring an accurate representation of the system dynamics. The accuracy of the reconstruction process depends on the quality (noise level) of the acquired data and the number of harmonic contributions considered. For numerical data without noise interference, the cross-correlation coefficient between the reconstructed signal and the well-sampled signal approaches 1 when all contributions of the response spectrum are considered. However, it may not be feasible to consider all harmonic contributions of the spectrum, necessitating the detection of relevant contributions or a specific frequency band of interest. For the system studied in this paper, the response of a semi-analytical model was downsampled at 20.6 Hz and reconstructed in the range of 10–120 Hz with an accuracy of 99.98%, as evaluated by the cross-correlation coefficient. For the real system response, downsampled by DIC at 23.7 Hz and reconstructed in the range of 12–144 Hz, the accuracy of the process was 99.3%, as evaluated by the cross-correlation coefficient between the high-frequency, high-precision LDV measurement and
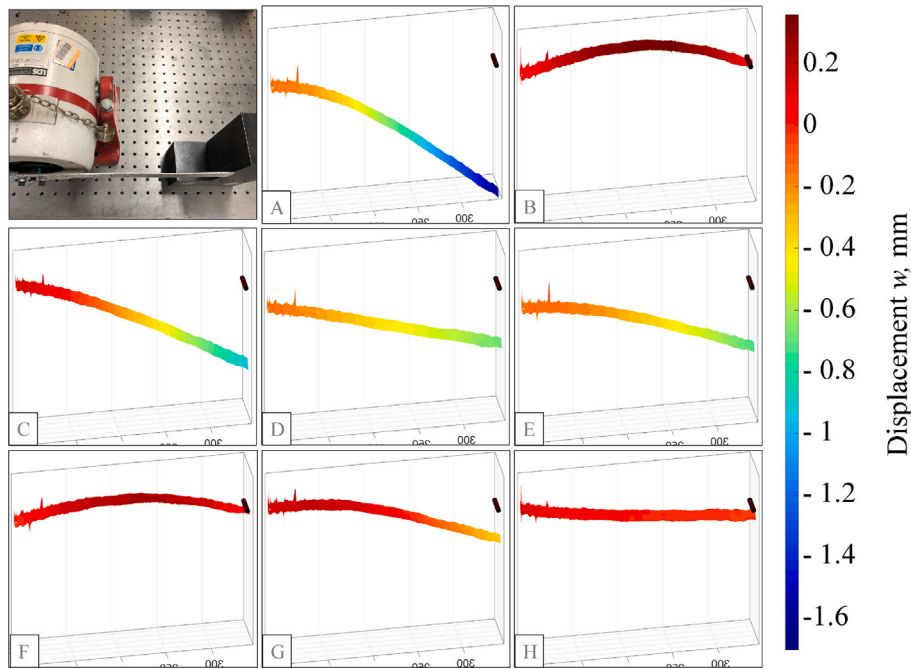
Fig. 14. Deformed shape of the beam measured by the DIC and SHA methods at different instants of time denoted by the letters A to H, as defined in Fig. 13. To highlight the deformed shape, the out-of-plane displacement w at each point was amplified by an 100 factor, while the true values are indicated by the color map. The black cylinder indicates the estimated position of the obstacle.

the reconstructed signal. Consequently, the presented methodology results in accurate full-field analysis that allows tracking the deformed shape of nonlinear structures that exhibits periodic motion at any time within the vibration period.

In summary, the results of the analysis conducted in this paper allow the following conclusions to be drawn.

- The time history of the displacements of a nonlinear system can also be recovered for downsampled signals using the DIC and SHA method.
- Comparison of the displacement measured with an LDV (high frequency and high precision measurement) on a reference point and the displacement recovered on the same point through SHA demonstrated the accuracy of the proposed method.
- The main limitation of this method might seem to be the knowledge of the main harmonics of the response. In the bench mark used to assess the method the response consisted of superharmonics and subharmonics of the exciting load, and this is the general behavior in nonlinear structure, so the method can be easily applied.
- The proposed methodology can be effectively applied even in operational conditions where measuring excitation forces and predicting the significant harmonic contribution of the structure's periodic response might be difficult. This can be achieved by exploiting high-frequency single-point measurement devices (microphone, strain gauge, accelerometer, others) to detect the significant harmonic frequencies, which can then be used for recovering the full-field displacements of the entire structure.

CRediT authorship contribution statement

Daniele Botto: Writing – review & editing, Supervision, Conceptualization. **Serena Occhipinti:** Writing – review & editing, Writing – original draft, Software, Investigation, Data curation. **Christian Maria Firrone:** Writing – review & editing, Supervision, Methodology. **Paolo Neri:** Writing – review & editing, Supervision, Methodology.

Declaration of competing interest

The corresponding author declares that this manuscript is original, has not been published before and is not currently being considered for publication elsewhere.

The corresponding author confirms that the manuscript has been read and approved by all named authors and that there are no other persons who satisfied the criteria for authorship but are not listed. The corresponding author further confirms that the order of authors listed in the manuscript has been approved by all of us.

The corresponding author is the sole contact for the Editorial process and is responsible for communicating with the other authors about progress, submissions of revisions and final approval of proofs.

Data availability

Data will be made available on request.

Acknowledgment

All authors approved the version of the manuscript to be published.

References

[1] D. Lezhin, S. Falaleev, A. Safin, A. Ulanov, D. Vergnano, Comparison of different methods of non-contact vibration measurement, Procedia Eng. 176 (2017) 175–183, http://dx.doi.org/10.1016/j.proeng.2017.02.286.

[2] L. Bertini, P. Neri, C. Santus, A. Guglielmo, Automated experimental modal analysis of bladed wheels with an anthropomorphic robotic station, Exp. Mech. 57 (2) (2016) 273–285, http://dx.doi.org/10.1007/s11340-016-0223-5.

[3] B. Halkon, S. Rothberg, Vibration measurements using continuous scanning laser vibrometry: Advanced aspects in rotor applications, Mech. Syst. Signal Process. 20 (6) (2006) 1286–1299, http://dx.doi.org/10.1016/j.ymssp.2005.11.009.

[4] M.N. Helfrick, C. Niezrecki, P. Avitabile, T. Schmidt, 3D digital image correlation methods for full-field vibration measurement, Mech. Syst. Signal Process. 25 (3) (2011) 917–927, http://dx.doi.org/10.1016/j.ymssp.2010.08.013.

[5] K. Zaletelj, J. Slavič, M. Boltežar, Full-field DIC-based model updating for localized parameter identification, Mech. Syst. Signal Process. 164 (2022) 108287, http://dx.doi.org/10.1016/j.ymssp.2021.108287.

[6] P.L. Reu, D.P. Rohe, L.D. Jacobs, Comparison of DIC and LDV for practical vibration and modal measurements, Mech. Syst. Signal Process. 86 (2017) 2–16, http://dx.doi.org/10.1016/j.ymssp.2016.02.006.

[7] A. Molina-Viedma, L. Felipe-Sesé, E. López-Alba, F. Díaz, 3D mode shapes characterisation using phase-based motion magnification in large structures using stereoscopic DIC, Mech. Syst. Signal Process. 108 (2018) 140–155, http://dx.doi.org/10.1016/j.ymssp.2018.02.006.

[8] D. Botto, M. Glorioso, S. Occhipinti, F. Cuccovillo, Uncertainty in identifying contact stiffness in a dovetail attachment for turbine blades, Mech. Syst. Signal Process. 197 (2023) 110379, http://dx.doi.org/10.1016/j.ymssp.2023.110379.

[9] L. Pesaresi, M. Stender, V. Ruffini, C.W. Schwingshackl, DIC measurement of the kinematics of a friction damper for turbine applications, in: Dynamics of Coupled Structures, Vol. 4, Springer International Publishing, 2017, pp. 93–101.

[10] R. Chabrier, E. Sadoulet-Reboul, G. Chevallier, E. Foltête, T. Jeannin, Full-field measurements with digital image correlation for vibro-impact characterisation, Mech. Syst. Signal Process. (2021) http://dx.doi.org/10.1016/j.ymssp.2021.107658.

[11] E. Ukshini, J. Dirckx, Non-linear saxophone reed vibrations measured by stroboscopic digital image correlation, in: ISMA 2020, 2020.

[12] K. Iijima, C. Ma, A.R. Pambela, T. Maeda, DIC measurement of deflection waves travelling along a thin flexural plate floating at water surface, Ocean Eng. 266 (2022) 113079, http://dx.doi.org/10.1016/j.oceaneng.2022.113079, URL: https://www.sciencedirect.com/science/article/pii/S0029801822023629.

[13] D.A. Ehrhardt, M.S. Allen, S. Yang, T.J. Beberniss, Full-field linear and nonlinear measurements using continuous-scan laser Doppler vibrometry and high speed three-dimensional digital image correlation, Mech. Syst. Signal Process. 86 (2017) 82–97, http://dx.doi.org/10.1016/j.ymssp.2015.12.003.

[14] J. Javh, J. Slavič, M. Boltežar, High frequency modal identification on noisy high-speed camera data, Mech. Syst. Signal Process. 98 (2018) 344–351, http://dx.doi.org/10.1016/j.ymssp.2017.05.008.

[15] W. Chen, M. Jin, I. Lawal, M.R. Brake, H. Song, Measurement of slip and separation in jointed structures with non-flat interfaces, Mech. Syst. Signal Process. 134 (2019) 106325, http://dx.doi.org/10.1016/j.ymssp.2019.106325.

[16] W. Chen, D. Jana, A. Singh, M. Jin, M. Cenedese, G. Kosova, M.R. Brake, C.W. Schwingshackl, S. Nagarajaiah, K.J. Moore, J.-P. Noël, Measurement and identification of the nonlinear dynamics of a jointed structure using full-field data, Part I: Measurement of nonlinear dynamics, Mech. Syst. Signal Process. 166 (2022) 108401, http://dx.doi.org/10.1016/j.ymssp.2021.108401.

[17] M. Jin, G. Kosova, M. Cenedese, W. Chen, A. Singh, D. Jana, M.R. Brake, C.W. Schwingshackl, S. Nagarajaiah, K.J. Moore, J.-P. Noël, Measurement and identification of the nonlinear dynamics of a jointed structure using full-field data; Part II - Nonlinear system identification, Mech. Syst. Signal Process. 166 (2022) 108402, http://dx.doi.org/10.1016/j.ymssp.2021.108402.

[18] H. Li, P. Wanchoo, A. Shukla, D. Chelidze, Smooth mode decomposition: Theory and its applications in full-field output-only modal analysis, Mech. Syst. Signal Process. 200 (2023) 110541, http://dx.doi.org/10.1016/j.ymssp.2023.110541.

[19] P. Neri, Frequency-band down-sampled stereo-DIC: Beyond the limitation of single frequency excitation, Mech. Syst. Signal Process. 172 (2022) 108980, http://dx.doi.org/10.1016/j.ymssp.2022.108980.

[20] L. Ruixin, Z. Sheng, B. Chen, Z. Gao, Y. Fu, Modal shapes measurements of a rotating disc using stroboscopic 3D digital image correlation and down-sampling strategy, in: C. Zuo, H. Wang, S. Feng, Q. Kemao (Eds.), International Conference on Optical and Photonic Engineering (IcOPEN 2022), SPIE, 2023, http://dx.doi.org/10.1117/12.2667027.

[21] S. Occhipinti, P. Neri, C.M. Firrone, D. Botto, Analysis of nonlinear vibrations using DIC and the smoothed harmonics method, in: Advances in Nonlinear Dynamics, Vol. I, Springer Nature Switzerland, 2024, pp. 691–701, http://dx.doi.org/10.1007/978-3-031-50631-4_58.

[22] B.A. Furman, B.D. Hill, J.R. Rigby, J.M. Wagner, R.B. Berke, Sensor synchronized DIC: A robust approach to linear and nonlinear modal analysis using low frame rate cameras, J. Sound Vib. 584 (2024) 118478, http://dx.doi.org/10.1016/j.jsv.2024.118478.

[23] Y. Dong, B. Pan, A review of speckle pattern fabrication and assessment for digital image correlation, Exp. Mech. 57 (8) (2017) 1161–1181, http://dx.doi.org/10.1007/s11340-017-0283-1.

[24] R. Bigger, B.t. Blaysat, C. Boo, M. Grewer, J. Hu, A. Jones, M. Klein, K. Raghavan, P. Reu, T. Schmidt, T. Siebert, M. Simenson, D. Turner, A. Vieira, T. Weikert, A Good Practices Guide for Digital Image Correlation, Jones, Elizabeth and Iadicola, Mark, 2018, http://dx.doi.org/10.32720/idics/gpg.ed1.

[25] R. Hartley, A. Zisserman, Multiple View Geometry in Computer Vision, Cambridge University Press, 2004, http://dx.doi.org/10.1017/cbo9780511811685.

[26] T.M. Inc., Computer vision toolbox, 2023, URL: https://www.mathworks.com.

[27] J. Blaber, B. Adair, A. Antoniou, Ncorr: Open-source 2D digital image correlation matlab software, Exp. Mech. 55 (6) (2015) 1105–1122, http://dx.doi.org/10.1007/s11340-015-0009-1.

[28] P. Neri, A. Paoli, A.V. Razionale, C. Santus, Low-speed cameras system for 3D-DIC vibration measurements in the kHz range, Mech. Syst. Signal Process. 162 (2022) 108040, http://dx.doi.org/10.1016/j.ymssp.2021.108040.

[29] M.T. Endo, A.N. Montagnoli, R. Nicoletti, Measurement of shaft orbits with photographic images and sub-sampling technique, Exp. Mech. 55 (2) (2014) 471–481, http://dx.doi.org/10.1007/s11340-014-9951-6.

[30] G. Strang, Linear Algebra and its Applications, Brooks Cole, 2005, p. 544.

[31] M. Legrand, S. Junca, S. Heng, Nonsmooth modal analysis of a N-degree-of-freedom system undergoing a purely elastic impact law, Commun. Nonlinear Sci. Numer. Simul. 45 (2017) 190–219, http://dx.doi.org/10.1016/j.cnsns.2016.08.022.

[32] F.C. Moon, S.W. Shaw, Chaotic vibrations of a beam with non-linear boundary conditions, Int. J. Non-Linear Mech. 18 (6) (1983) 465–477, http://dx.doi.org/10.1016/0020-7462(83)90033-1.

[33] S. Shaw, Forced vibrations of a beam with one-sided amplitude constraint: Theory and experiment, J. Sound Vib. 99 (2) (1985) 199–212, http://dx.doi.org/10.1016/0022-460x(85)90357-8.

[34] P. Neri, B. Peeters, Non-harmonic Fourier analysis for bladed wheels damage detection, J. Sound Vib. 356 (2015) 181–194, http://dx.doi.org/10.1016/j.jsv.2015.06.048.

[35] T. Yoshizawa, S. Hirobayashi, T. Misawa, Noise reduction for periodic signals using high-resolution frequency analysis, Eurasip J. Audio Speech 2011 (1) (2011) http://dx.doi.org/10.1186/1687-4722-2011-426794.